ARTICLE

First-Principles Thermodynamics Study of CO/OH Induced Disintegration of Precious Metal Nanoparticles on TiO_2(110)

Shiyan Cao, Sulei Hu*, Wei-Xue Li*

Department of Chemical Physics, School of Chemistry and Materials Science, Hefei National Research Center for Physical Sciences at the Microscale, University of Science and Technology of China, Hefei 230026, China

(Dated: Received on July 12, 2022; Accepted on September 1, 2022)

Revealing the fundamental mechanisms governing reactant-induced disintegration of supported metal nanoparticles and their dependences on the metal component and reactant species is vital for improving the stability of supported metal nanocatalysts and single-atom catalysts. Here we use first-principles-based disintegration thermodynamics to study the CO- and OH- induced disintegration of Ag, Cu, Au, Ni, Pt, Rh, Ru, and Ir nanoparticles into metal-reactant complexes ($M(CO)_n$, $M(OH)_n$, n=1 and 2) on the pristine and bridge oxygen vacancy site of TiO_2(110). It was found that CO has a stronger interaction with these considered transition metals compared to OH, resulting in lower formation energy and a larger promotion effect on the disintegration of nanoparticles (NPs). The corresponding reactant adsorption energy shows a linear dependence on the metal cohesive energy, and metals with higher cohesive energies tend to have higher atomic stability due to their stronger binding with reactant and support. Further disintegration free energy calculations of NPs into metal-reactant complexes indicate only CO-induced disintegration of Ni, Rh, Ru, and Ir nanoparticles is thermodynamically feasible. These results provide a deeper understanding of reactant-induced disintegration of metal nanoparticles into thermodynamically stable metal single-atom catalysts.

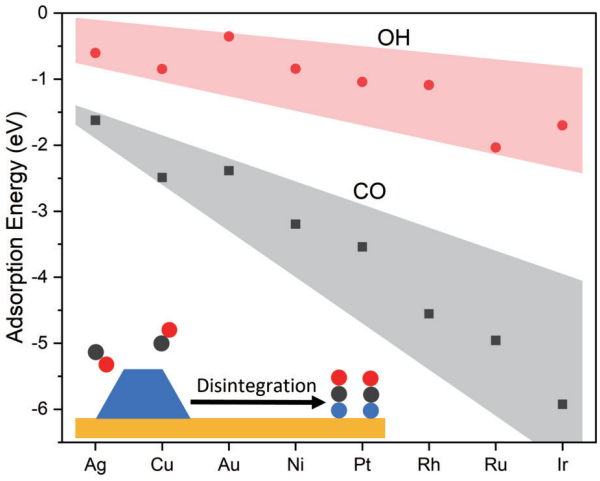

Key words: Thermodynamics, Disintegration, Density functional theory, Metal nanoparticle

I. INTRODUCTION

Keeping the operando stability and flexibility of highly active metal nanoparticles (NPs) and even single-atom catalysts (SACs) is crucial for energy and environmental sustainment [1–5]. Under reaction conditions, these nanocatalysts are highly dynamic and may grow in size through Ostwald ripening mechanisms [6–10] or disintegrate into smaller clusters or even single atoms [11, 12]. The SACs, which have high atomic efficiency and well-defined active sites, also tend to aggregate via reactant-assisted nucleation and growth [13–19]. Revealing the underlying fundamental mechanisms governing reactant-induced disintegration of metal nanoparticles during the reaction remains an issue to maintain the long-term stability of these catalysts.

* Authors to whom correspondence should be addressed. E-mail: husulei@ustc.edu.cn, wxli70@ustc.edu.cn

Thermodynamically, disintegration occurs when the metal atoms have stronger bindings with surface sites or the reactant ligands, compared to the metal-metal bindings in the NPs [11, 20–23]. Disintegration greatly relies on the temperature or the reactant, which may tweak the composition and structures of the support [23, 24] or even reverse the metal atoms back to the larger NPs [25, 26]. The metal-support-reactant interplay of the SACs is vital for their trapping, stabilization, and manipulation of the corresponding electronic structures [27–30]. Such interplay further involves the strain of core-shell structure [31, 32], reactant-induced structural distortions [16], and coordination atoms adjustment [33]. Nevertheless, a deeper understanding of the disintegration of NPs and the stability of SACs under reaction conditions, especially the dependence on metal-reactant interaction, is still highly desired for improving the stability of these nanocatalysts.

In this work, we studied the effects of the reactant, metal, and support defect on NPs disintegration. Density functional theory (DFT) calculation was performed for the surface monomers formation and NPs disintegration of eight metals (M=Ni, Cu, Ag, Au, Pt, Rh, Ru, and Ir) and their metal-reactant complex ($M(CO)_n$ and $M(OH)_n$, n=1, 2) on pristine and oxygen vacancy defective rutile TiO_2(110). It shows the disintegration of NPs of these metals on TiO_2(110) is not thermodynamically favored under an inert or H_2O atmosphere, regardless of the pristine or defective surface. In contrast, under CO conditions, the disintegration of NPs and the formation of single metal atoms is more favored, probably due to the stronger adsorption energies of CO on supported metal atoms. As a comparison, metals with higher cohesive energies generally show higher single atom aggregation resistance under reaction conditions, because of the stronger binding between the metal atom and reactant molecules.

II. METHODS

The Vienna *Ab initio* Simulation Package (VASP 5.4) [34] was used with the projector-augmented wave method [35] and Perdew-Burke-Ernzerhof (PBE) functional [36] for all calculations. The cutoff energy of the plane wave basis set was set to 400 eV. The spin polarization was considered. Monkhorst-Pack k-points were set to 3×3×1. Systems were relaxed until the force on each atom was less than 0.02 eV/Å. Optimized rutile (110) parameters were a=4.598 Å, c=2.958 Å, which match well with experimental values a=4.593 Å, c=2.959 Å [37]. In this work, we used experimental cohesive energies [38] for the supported metal atoms and complexes.

Adsorption structures on rutile (110) were described by a (2×4) slab with a 15 Å vacuum layer. Four Ti-O layers were used and the top two were relaxed for optimization while the bottom two were fixed, and dipole correction was considered. Various adsorption sites of surface metal atoms or complexes on the pristine surface were considered and illustrated in FIG. S1 in Supplementary materials (SM). The preferred sites are listed in Table S1 in SM. For the defective rutile (110) surface, the surface bridge oxygen vacancies were considered and the spatial distribution was evaluated (see details in SM). In this work, one surface bridge oxygen atom was removed from each supercell, leading to a 1/8 oxygen vacancy coverage. Monkhorst-Pack k-points were set to 3×3×1. Systems were relaxed until the force on each atom was less than 0.02 eV/Å.

The effect of Hubbard U correction was evaluated. At $U_{\text{eff}} = U - J = 3$ eV, the formation energy increases with a maximum of 0.22 eV on rutile (110). Because this value was small compared to the difference between metals (2.66 eV of the formation energy difference between Ir and Ni), the Hubbard U correction was not considered in this work. For the formation energy of a metal atom or metal-reactant complexes, the experimental metal cohesive energies [38] were used.

III. RESULTS AND DISCUSSION

A. Formation energy

The aggregation of the supported metal atoms and disintegration of the NPs into dispersed species mainly rely on the interplay of the supported metal atoms, reactants, and support [39]. Analyzing this interplay to stabilize the supported metal atoms and NPs requires to calculate the structures and energies of the dispersed species. In this work, we focus on surface monomers MX_n which contains only one metal atom, and X is the reactant ligand.

Under reaction conditions, a surface monomer is formed when the metal atom detaches from metal NPs via the metal-reactant complex and adsorbs on the support surface. The corresponding energy change is the formation energy E_f and defined as:

DOI: 10.1063/1674-0068/cjcp2207111

$$E_f = E_{slab}(MX_n) - E_{slab}(oxide) - E_B(M) - n \times E(X) \quad (1)$$

where $E_{slab}(MX_n)$, $E_{slab}(oxide)$, $E_B(M)$, and $E(X)$ are the total energies of the surface monomers MX_n on the oxide surface, the slab of the oxide surface, a bulk metal atom, and the gaseous reactant. Since OH is not stable as a standalone molecule, we use gaseous H_2O and H_2 as references.

The structures and energies of surface monomers are calculated for eight transition metals (M=Ag, Cu, Au, Ni, Rh, Pt, Ru, and Ir) and their reactant complex MX_n (n=1, 2; X=CO and OH) on pristine TiO_2(110). Various possible adsorption sites on the pristine surface are considered and shown in SM. The corresponding E_f are shown in FIG. 1, where metals in the x-axis are in ascending cohesive energy (E_{coh}). As a typical case, E_f for Au atom reaches 3.42 eV (black bar), indicating that individual Au atoms are difficult to be formed without reactant. When CO is introduced, the corresponding E_f drops to 1.03 eV (red bar in FIG. 1(a)), which suggests that CO can greatly induce the formation of Au species in the form of AuCO. When the ligand turns to OH, E_f of AuOH becomes 3.07 eV (red bar in FIG. 1(b)), which is only 0.35 eV lower than that of Au. This small change shows that OH can barely induce the formation of Au monomers.

Similarly, for other metals, their E_f values without reactant are all higher than 1.5 eV (black bars), which shows that they are difficult to be formed without the help of reactant. Introducing the CO (FIG. 1(a)) or OH (FIG. 1(b)), the average drop values of E_f are 2.39 eV and 0.75 eV, respectively. This result shows that both reactants can induce the formation of metal-reactant complexes and the formation of CO complexes is more favored than OH complexes, while metal NPs under the CO atmosphere become more vulnerable than H_2O conditions on pristine TiO_2(110). From FIG. 1(a), metal atoms binding with two CO ligands show a lower and usually negative E_f than that with one CO, and Ag and Ru have the highest positive E_f (1.00 eV) and the lowest negative E_f (−1.83 eV) in form of $M(CO)_2$, repectively. Comparing FIG. 1 (a) and (b), the E_f values of M(OH) and $M(OH)_2$ do not show apparent differences under the OH environment and all are positive, indicating OH cannot facilitate the formation of a single metal atom. Even a higher E_f (3.62 eV, blue bar in FIG. 1(b)) is found for $Au(OH)_2$, compared to AuOH (3.12 eV) and Au (3.43 eV). Metal monomers, such as $Au(CO)_2$ or $Pt(CO)_2$, cannot stably adsorb on TiO_2(110), which is consistent with the detachment observed in the *ab initio* molecular dynamics study [40].

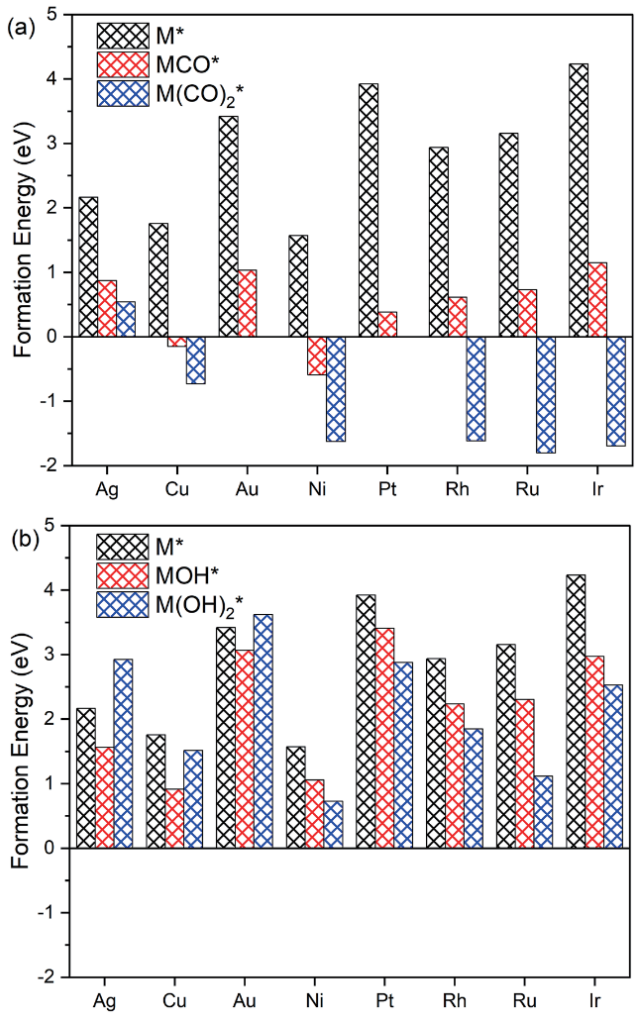

FIG. 1 Formation energies of metal atoms or complexes on the pristine surface under (a) CO and (b) H_2O environments (OH).

The formation energy includes two contributions at the same time, one is that the metal atoms lose their bonds with surrounding atoms, and the other is the formation of new bonds with the support and reactants. To more clearly see the contribution of the reactants and to understand the underlying determinants, we calculate the reactant adsorption energy (E_{ads}), which measures the energy change of the reactant adsorbing on the supported metal atom:

$$E_{ads} = E_{slab}(MX_n) - E_{slab}(M) - n \times E(X) \quad (2)$$

where $E_{slab}(M)$ is the total energies of surface single metal atoms on the oxide surface. A lower (negative) E_{ads} represents a stronger binding between reactant

DOI: 10.1063/1674-0068/cjcp2207111

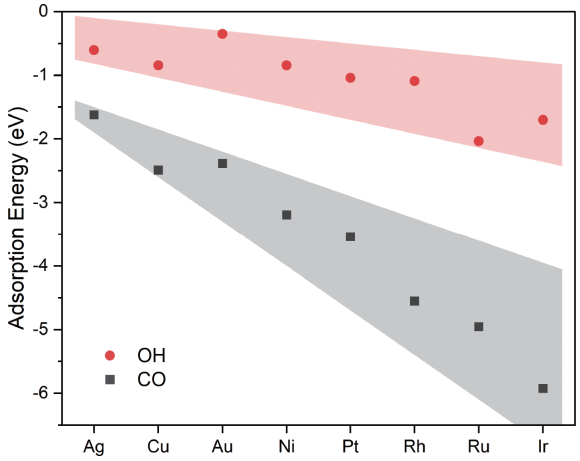

FIG. 2 The reactant adsorption energy of different monomers on the pristine surface. For a given metal-reactant combination, the corresponding adsorption energy is determined by the lower value between that of MX and MX_2 (M=metal, X=OH or CO).

and metal atoms. FIG. 2 shows how E_{ads} changes with different metals on the pristine surface. For each metal M and reactant X combination, we choose the lower E_{ads} between MX and MX_2. As shown in FIG. 2, all monomers have negative E_{ads} on the pristine surface, indicating the reactants bind with all the metal atoms and facilitate the formation of the corresponding metal-reactant complexes. As E_{coh} of metals increases (from Ag to Ru), E_{ads} becomes more negative for both CO and OH. This result suggests that the binding between reactant and metal atom is stronger for metals with a higher E_{coh}. As a result, metals with a high E_{coh} tend to combine with more ligand molecules, compared to low E_{coh} metals. The metal-reactant complexes of OH and CO can be divided into two bands in FIG. 2 and the complexes with OH (in red band) have a lower $|E_{ads}|$ than that with CO (in grey band). This difference shows that binding between metal atoms and OH is much weaker compared to those with CO, which is consistent with the result that CO has a relatively good stabilizing effect on metal single atoms compared to OH, as revealed in FIG. 1.

Under reducing atmospheres, oxygen vacancies may form and stabilize these dispersed metal-reactant complexes [40, 41]. Among the different oxygen vacancies of TiO_2(110) considered, the bridging oxygen vacancy is energetically the most favorable. On the bridging oxygen vacancies, we calculate the structures and formation energies of these eight metal monomers, as shown in FIG. 3(a) (CO) and FIG. 3(b) (OH). Without reactant, the introduction of vacancies reduces E_f of metal

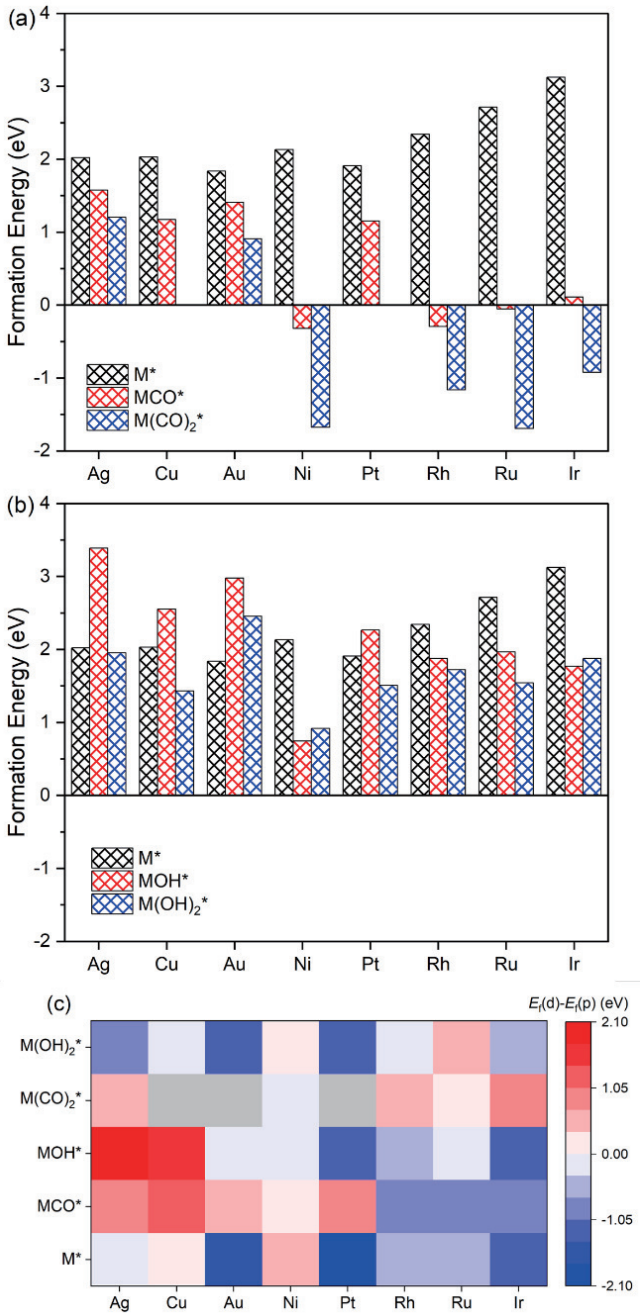

FIG. 3 Formation energies of metal atoms or complexes on the bridging oxygen vacancy of TiO_2(110) surface under (a) CO, and (b) H_2O (OH). (c) Heatmap of the formation energy difference between the pristine and defective surface. For the formation energy difference, red or blue squares represent that monomers have lower formation energy on the pristine or defective surface; grey squares represent that the monomer detaches from the surface during structure relaxation.

atoms (black bars) by an average value of 0.63 eV compared to the pristine surface of TiO_2(110). This result suggests that the additional coordination provided by the vacancies is indeed beneficial for lowering the ener-

DOI: 10.1063/1674-0068/cjcp2207111

gy of individual metal atoms. However, the contribution of this coordination (0.63 eV) is limited, compared to the energy reduction brought about by reactant adsorption on the pristine TiO_2(110) surface (the decrement of E_f is 2.39 eV for CO and 0.75 eV for OH in FIG. 1). When CO and OH are involved, the average E_f of all metals further drops from 2.26 eV (black bars) to 0.59 eV (MCO, red bars in FIG. 3(a)) and 2.19 eV (MOH, red bars in FIG. 3(b)). Such difference shows that CO complexes are more favored to form than OH on the defective surface, similar to that on the pristine surface.

To specifically show the influence of oxygen vacancies on E_f of metal under CO and H_2O environment, the difference of E_f between pristine and defective surfaces is shown in FIG. 3(c). Red or blue squares in FIG. 3(c) represent a higher or a lower E_f on the defective surface than that on the pristine surface respectively, grey squares represent that monomers are thermodynamically unstable on either surface. Most metals (M^*) have a decreasing E_f (blue squares) at the vacancy sites, compared to the pristine surface. We note that Cu and Ni have an increasing E_f and the metal atoms tend to stay at the bridge oxygen site even if oxygen vacancies exist, which may be attributed to the stronger charge transfer between these metal atoms and the bridge oxygen atoms of the rutile surface [42]. For metal-reactant complexes, Pt, Rh, Ru, and Ir (right half, high E_{coh}) show a lower E_f values than Ag, Cu, Au, and Ni (left half, low E_{coh}). This contrast suggests that the oxygen vacancies have a stronger stabilization effect if their metals have a higher E_{coh}, considering these metal atoms require more and stronger surface coordination and reactant ligands to become stable when they detach from NPs and lose their surrounding coordinating metal atoms. We also calculate the reactant adsorption energy on the defective surface and plot them in FIG. S3 in SM. Results indicate on the defective surface, adsorption of the reactant on most metal atoms (except Ni) is weaker than those on the pristine surface. This difference is because additional coordination and stronger charge transfer of the oxygen vacancy with metal atoms decrease the capability of the metal atoms to bind with the reactant molecules.

To provide more chemical insight, the crystal orbital overlap population (COOP) is calculated for $Rh(CO)_2$* and $Rh(OH)_2$* on both pristine and defective TiO_2(110), as shown in FIG. S6 in SM. The integrated COOP (ICOOP) up to the Fermi level is also calculated to evaluate the bonding strength. For $Rh(CO)_2$* on the pristine surface, most antibonding states are unoccupied, leading to a strong binding between CO and Rh. For $Rh(CO)_2$* on the defective surface, the antibonding state is largely occupied and the ICOOP value decreases from 0.158 to 0.077. This suggests that the existence of oxygen vacancies greatly weakens the bonding between Rh metal atoms and reactant CO. For the $Rh(OH)_2$*, the antibonding are largely occupied on both pristine and defective surface and OH barely stabilizes the Rh atoms, which also matches well with the thermodynamic results.

B. Disintegration free energy

If the surface monomer is thermodynamically stable compared to metal NPs, the disintegration of NPs occurs. To access the improvement of the reactant on the NPs disintegration, we calculate the disintegration Gibbs free energy of the complex MX_n (X=CO or OH, n=1 or 2) [22]:

$$\Delta G_{dis}(R,T,p) = E_f - n \times \Delta\mu_X(T,p) - \Delta E_{NP}(R) - TS \tag{3}$$

where T and R are the temperature and radius of the particles. $\Delta E_{NP}(R) = (3\gamma\Omega)/R$ is the energy difference between the given NP and the bulk metals, where γ and Ω are surface energy and molar volume of bulk metals. $\Delta\mu_X$ is the chemical potential of the reactant molecule in the gas phase:

$$\Delta\mu_X(T,p) = \Delta\mu_X(T,p_0) + kT\ln\left(\frac{p}{p_0}\right) \tag{4}$$

where $\Delta\mu_X(T,p_0)$ is the chemical potential of reactant X at T and standard pressure p_0, which is obtained from ASE library [43], and p is the partial pressure of the reactant. S is the configurational entropy of the complexes on the surface. As a typical example, for a 0.01 coverage of the complexes, the estimated entropy contribution is $4.83\times10^{-4}T$ (in eV) [44].

ΔG_{dis} describes the energy difference of the surface monomer with respect to the NP. A negative ΔG_{dis} indicates that the disintegration of the given sized particles is thermodynamically favorable under a given T and p. To evaluate the environmental contribution to ΔG_{dis}, FIG. 4(a) shows how ΔG_{dis} of NiCO changes with T, p, and particle size. When T decreases from

DOI: 10.1063/1674-0068/cjcp2207111

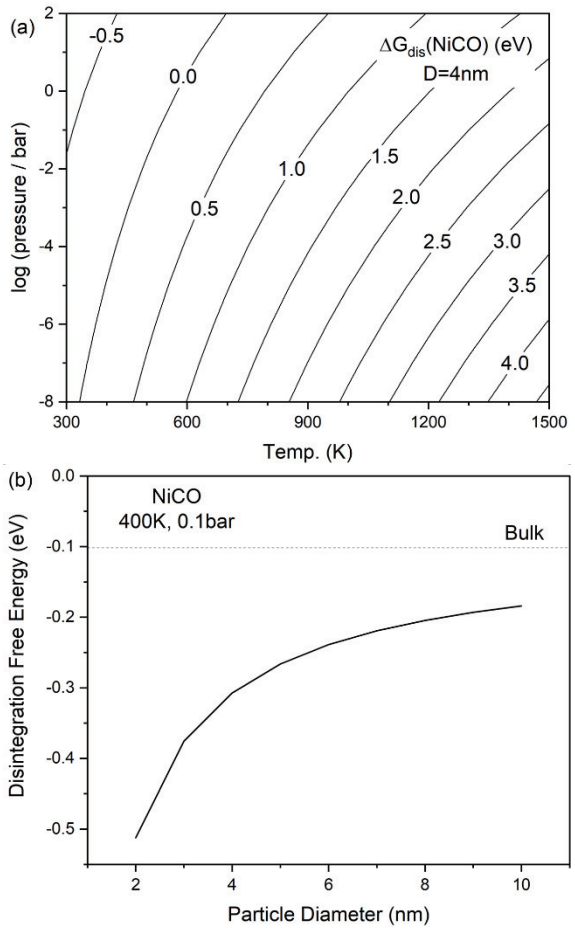

FIG. 4 Temperature, pressure, and particle size effect on the disintegration free energy. (a) Contour plot of disintegration free energy of 4 nm Ni particles *vs.* temperature and CO pressure. (b) Disintegration free energy of Ni NPs *vs.* the particle size. The dashed line represents the energy of the bulk Ni.

1500 K to 300 K and p increases from 10^{-8} bar to 10^{2} bar, $\Delta G_{\rm dis}$ decreases more than 4 eV. This suggests that the disintegration behavior largely depends on the actual reaction conditions; and in order to induce the disintegration of NPs, lower T and high p are more favored. For the particle size effect, FIG. 4(b) shows that $\Delta G_{\rm dis}$ decreases drastically below 4 nm and the difference between the bulk metals and 10 nm NPs is about 0.1 eV. This indicates that small NPs are more likely to be disintegrated into monomers and large particles have only minor differences compared to that of bulk metals. Experimental observations also show that a higher reactant pressure and lower temperature favor the disintegrations of Cu and Rh, and the dispersed metal can reform larger particles under higher temperatures [45, 46].

We then move to the disintegration behavior of different metal nanoparticles. FIG. 5 shows $\Delta G_{\rm dis}$ of surface monomers of different metals on perfect and defective surfaces. The T, p, and particle sizes are set to 400 K, 0.1 bar, and 4 nm. For all the metals we considered, only Ni, Rh, Ru, and Ir have negative $\Delta G_{\rm dis}$ on both pristine and defective surfaces, which shows that only these metals can be dispersed into single atoms on the pristine surface under such conditions. Compared to non-reactant conditions, when CO is involved the decrement of $\Delta G_{\rm dis}$ is up to 3.45 eV (from Ir to $Ir(CO)_2$), while for OH this value is only 1.42 eV (from Ru to $Ru(OH)_2$). The monomers of CO (red circles) also have lower $\Delta G_{\rm dis}$ than that of OH (blue triangles). This indicates that CO is a good reactant for the disintegration of the NPs and stabilization of the SACs on TiO_2(110), compared to OH. This reactant stabilization effect dominates even when oxygen vacancy is involved, where $\Delta G_{\rm dis}$ of monomers at the pristine surface (red solid circles) is lower or slightly higher (0.08 eV) than that at the defective surface (red hollow circles). For other metal-reactant combinations which have positive $\Delta G_{\rm dis}$, although the introduction of the reactant still induces the formation of the metal-reactant complexes, the monomers are thermodynamically unstable on the TiO_2(110) compared to the NPs. These monomers tend to recombine with NPs and other processes, such as Ostwald ripening, may happen. This result gives valuable suggestions about tuning the stabili-

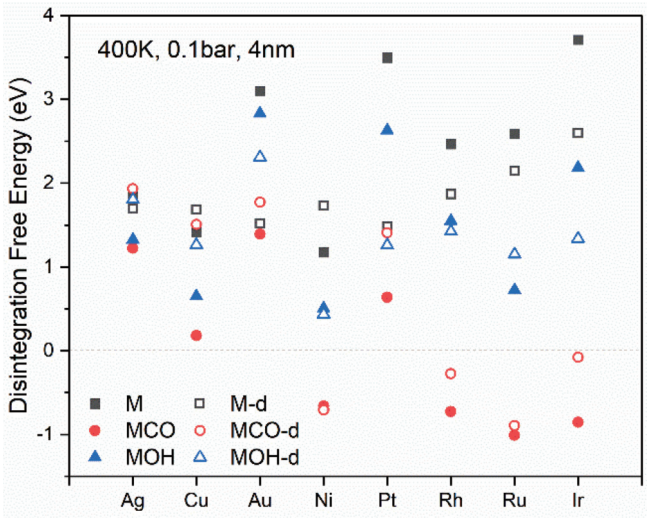

FIG. 5 Disintegration free energy of different surface monomers on rutile (110). The lower energy is chosen for monomers between MX and MX_2 (M=metal, X=CO and OH). Solid and hollow symbols represent the energies on pristine and defective surfaces. The temperature, pressure, and particle size are set to 400 K, 0.1 bar, and 4 nm, respectively.

DOI: 10.1063/1674-0068/cjcp2207111

ty of the nanocatalysts with the impact of defects and reactants.

IV. CONCLUSION

We used first-principles thermodynamics calculations to study the disintegration of eight transition metals (Ag, Cu, Au, Ni, Rh, Pt, Ru, and Ir) into metal-reactant complex MX_n (n=1, 2; X=CO, OH) on rutile TiO_2(110) surface. It shows that CO can effectively disperse Ni, Rh, Ru, and Ir nanoparticles thermodynamically, due to its strong binding with supported metal atoms, compared to OH. Metals with higher cohesive energies tend to have a higher atomic aggregation-resistance stability due to their stronger binding with reactant and support. This work provides a valuable understanding of the disintegration of metal nanoparticles, as well as the preparation of stable single-atom catalysts.

Supplenmentary materials: Additional figures and tables illustrating benchmarks of the energies, distributions of oxygen vacancies, adsorption sites of monomers, and disintegration free energies under different conditions are available.

V. ACKNOWLEDGMENTS

This work was supported by the National Key R&D Program of China (2021YFB3502000, 2018YFA0208603), National Program for Support of Top-notch Young Professional, Chinese Academy of Sciences Youth Innovation Promotion Association, Anhui Outstanding Youth Fund (No.2208085J27), the National Natural Science Foundation of China (No.22221003, No.91945302, No.21903077), the Strategic Priority Research Program of the Chinese Academy of Sciences (XDB0450102), Innovation Program for Quantum Science and Technology (2021ZD0303302), Chinese Academy of Sciences (QYZDJ-SSW-SLH054), K. C. Wong Education (GJTD-2020-15), the Dalian National Laboratory For Clean Energy (DNL) Cooperation Fund, the CAS (DNL201920) and the China Postdoctoral Science Foundation, the Fundamental Research Funds for the Central Universities, USTC Research Funds of the Double First-Class Initiative (KY9990000170, YD9990002008). The authors thank Supercomputing Center of University of Science and Technology of China and Hefei Advanced Computing Center.

[1] H. Goksu, N. Zengin, H. Burhan, K. Cellat, and F. Sen, Sci. Rep. **10**, 8043 (2020).
[2] A. Beniya and S. Higashi, Nat. Catal. **2**, 590 (2019).
[3] J. W. D. Ng, M. García-Melchor, M. Bajdich, P. Chakthranont, C. Kirk, A. Vojvodic, and T. F. Jaramillo, Nat. Energy **1**, 16053 (2016).
[4] J. A. Rodriguez, P. Liu, J. Hrbek, J. Evans, and M. Perez, Angew. Chem. Int. Ed. **46**, 1329 (2007).
[5] S. Hu and W. X. Li, Science **374**, 1360 (2021).
[6] W. Yuan, D. Zhang, Y. Ou, K. Fang, B. Zhu, H. Yang, T. W. Hansen, J. B. Wagner, Z. Zhang, Y. Gao, and Y. Wang, Angew. Chem. Int. Ed. Engl. **57**, 16827 (2018).
[7] G. S. Parkinson, Z. Novotny, G. Argentero, M. Schmid, J. Pavelec, R. Kosak, P. Blaha and U. Diebold, Nat. Mater. **12**, 724 (2013).
[8] L. Luo, M. H. Engelhard, Y. Shao, and C. Wang, ACS Catal. **7**, 7658 (2017).
[9] M. A. van Spronsen, J. W. M. Frenken, and I. M. N. Groot, Nat. Commun. **8**, 429 (2017).
[10] S. Cao, X. Chai, S. Hu, and W. X. Li, J. Phys. Chem. C **126**, 8056 (2022).
[11] S. Wei, A. Li, J. C. Liu, Z. Li, W. Chen, Y. Gong, Q. Zhang, W. C. Cheong, Y. Wang, L. Zheng, H. Xiao, C. Chen, D. Wang, Q. Peng, L. Gu, X. Han, J. Li, and Y. Li, Nat. Nanotechnol. **13**, 856 (2018).
[12] E. D. Goodman, A. C. Johnston-Peck, E. M. Dietze, C. J. Wrasman, A. S. Hoffman, F. Abild-Pedersen, S. R. Bare, P. N. Plessow, and M. Cargnello, Nat. Catal. **2**, 748 (2019).
[13] B. Qiao, A. Wang, X. Yang, L. F. Allard, Z. Jiang, Y. Cui, J. Liu, J. Li, and T. Zhang, Nat. Chem. **3**, 634 (2011).
[14] L. Nie, D. Mei, H. Xiong, B. Peng, Z. Ren, X. I. P. Hernandez, A. DeLaRiva, M. Wang, M. H. Engelhard, L. Kovarik, A. K. Datye, and Y. Wang, Science **358**, 1419 (2017).
[15] J. H. Fu, J. H. Dong, R. Si, K. J. Sun, J. Y. Zhang, M. R. Li, N. N. Yu, B. S. Zhang, M. G. Humphrey, Q. Fu, and J. Huang, ACS Catal. **11**, 1952 (2021).
[16] J. Hulva, M. Meier, R. Bliem, Z. Jakub, F. Kraushofer, M. Schmid, U. Diebold, C. Franchini, and G. S. Parkinson, Science **371**, 375 (2021).
[17] X. He, Q. He, Y. Deng, M. Peng, H. Chen, Y. Zhang, S. Yao, M. Zhang, D. Xiao, D. Ma, B. Ge, and H. Ji, Nat. Commun. **10**, 3663 (2019).
[18] H. Yang, L. Shang, Q. Zhang, R. Shi, G. I. N. Waterhouse, L. Gu, and T. Zhang, Nat. Commun. **10**, 4585 (2019).
[19] L. Lin, J. Liu, X. Liu, Z. Gao, N. Rui, S. Yao, F. Zhang, M. Wang, C. Liu, L. Han, F. Yang, S. Zhang, X. Wen, S. D. Senanayake, Y. Wu, X. Li, J. A. Rodriguez, and D. Ma, Nat. Commun. **12**, 6978 (2021).
[20] Y. Tang, C. Asokan, M. Xu, G. W. Graham, X. Pan, P. Christopher, J. Li, and P. Sautet, Nat. Commun.

DOI: 10.1063/1674-0068/cjcp2207111

10, 4488 (2019).
[21] Y. Q. Su, Y. Wang, J. X. Liu, I. A. W. Filot, K. Alexopoulos, L. Zhang, V. Muravev, B. Zijlstra, D. G. Vlachos, and E. J. M. Hensen, ACS Catal. **9**, 3289 (2019).
[22] R. Ouyang, J. X. Liu, and W. X. Li, J. Am. Chem. Soc. **135**, 1760 (2013).
[23] J. C. Liu, Y. G. Wang, and J. Li, J. Am. Chem. Soc. **139**, 6190 (2017).
[24] F. Wang, J. Ma, S. Xin, Q. Wang, J. Xu, C. Zhang, H. He, and X. C. Zeng, Nat. Commun. **11**, 529 (2020).
[25] M. Moliner, J. E. Gabay, C. E. Kliewer, R. T. Carr, J. Guzman, G. L. Casty, P. Serna, and A. Corma, J. Am. Chem. Soc. **138**, 15743 (2016).
[26] R. Li, X. Xu, B. Zhu, X. Y. Li, Y. Ning, R. Mu, P. Du, M. Li, H. Wang, J. Liang, Y. Chen, Y. Gao, B. Yang, Q. Fu, and X. Bao, Nat. Commun. **12**, 1406 (2021).
[27] K. Liu, X. Zhao, G. Ren, T. Yang, Y. Ren, A. F. Lee, Y. Su, X. Pan, J. Zhang, Z. Chen, J. Yang, X. Liu, T. Zhou, W. Xi, J. Luo, C. Zeng, H. Matsumoto, W. Liu, Q. Jiang, K. Wilson, A. Wang, B. Qiao, W. Li, and T. Zhang, Nat. Commun. **11**, 1263 (2020).
[28] R. Lang, W. Xi, J. C. Liu, Y. T. Cui, T. Li, A. F. Lee, F. Chen, Y. Chen, L. Li, L. Li, J. Lin, S. Miao, X. Liu, A. Wang, X. Wang, J. Luo, B. Qiao, J. Li, and T. Zhang, Nat. Commun. **10**, 234 (2019).
[29] L. DeRita, J. Resasco, S. Dai, A. Boubnov, H. V. Thang, A. S. Hoffman, I. Ro, G. W. Graham, S. R. Bare, G. Pacchioni, X. Pan, and P. Christopher, Nat. Mater. **18**, 746 (2019).
[30] H. B. Zhang, G. G. Liu, L. Shi, and J. H. Ye, Adv. Energy Mater. **8**, 1701343 (2018).
[31] Y. Yao, S. Hu, W. Chen, Z. Q. Huang, W. Wei, T. Yao, R. Liu, K. Zang, X. Wang, G. Wu, W. Yuan, T. Yuan, B. Zhu, W. Liu, Z. Li, D. He, Z. Xue, Y. Wang, X. Zheng, J. Dong, C. R. Chang, Y. Chen, X. Hong, J. Luo, S. Wei, W. X. Li, P. Strasser, Y. Wu, and Y. Li, Nat. Catal. **2**, 304 (2019).
[32] K. Jiang, M. Luo, Z. Liu, M. Peng, D. Chen, Y. R. Lu, T. S. Chan, F. M. F. de Groot, and Y. Tan, Nat. Commun. **12**, 1687 (2021).
[33] X. Li, H. Rong, J. Zhang, D. Wang, and Y. Li, Nano Res. **13**, 1842 (2020).
[34] G. Kresse and J. Hafner, Phys. Rev. B: Condens. Matter **47**, 558 (1993).
[35] G. Kresse and D. Joubert, Phys. Rev. B **59**, 1758 (1999).
[36] J. P. Perdew, K. Burke, and M. Ernzerhof, Phys. Rev. Lett. **77**, 3865 (1996).
[37] J. K. Burdett, T. Hughbanks, G. J. Miller, J. W. Richardson, and J. V. Smith, J. Am. Chem. Soc. **109**, 3639 (1987).
[38] C. Kittel, *Introduction to Solid State Physics*, 8th Edn., Hoboken, NJ: John Wiley & Sons, (2005).
[39] S. Hu and W. X. Li, ChemNanoMat **4**, 510 (2018).
[40] N. Humphrey, S. Bac, and S. Mallikarjun Sharada, J. Chem. Phys. **154**, 234709 (2021).
[41] J. Wan, W. Chen, C. Jia, L. Zheng, J. Dong, X. Zheng, Y. Wang, W. Yan, C. Chen, Q. Peng, D. Wang, and Y. Li, Adv. Mater. **30**, 1705369 (2018).
[42] D. Pillay, Y. Wang, and G. S. Hwang, Korean J. Chem. Engineer. **21**, 537 (2004).
[43] A. Hjorth Larsen, J. Jorgen Mortensen, J. Blomqvist, I. E. Castelli, R. Christensen, M. Dulak, J. Friis, M. N. Groves, B. Hammer, C. Hargus, E. D. Hermes, P. C. Jennings, P. B. Jensen, J. Kermode, J. R. Kitchin, E. L. Kolsbjerg, J. Kubal, K. Kaasbjerg, S. Lysgaard, J. B. Maronsson, T. Maxson, T. Olsen, L. Pastewka, A. Peterson, C. Rostgaard, J. Schiøtz, O. Schütt, M. Strange, K. S. Thygesen, T. Vegge, L. Vilhelmsen, M. Walter, Z. Zeng, and K. W. Jacobsen, J. Phys. Condens. Matter. **29**, 273002 (2017).
[44] K. Reuter and M. Scheffler, Phys. Rev. B **68**, 045407 (2003).
[45] B. Eren, D. Zherebetskyy, L. L. Patera, C. H. Wu, H. Bluhm, C. Africh, L. W. Wang, G. A. Somorjai, and M. Salmeron, Science **351**, 475 (2016).
[46] A. Berkó and F. Solymosi, J. Catal. **183**, 91 (1999).

DOI: 10.1063/1674-0068/cjcp2207111